Asia-Pacific Journal of Science and Technology :Volume : 27. Issue : 03. Article ID.: APST-27-03-09. Research Article

APST

Asia-Pacific Journal of Science and Technology

https//:www.tci-thaijo.org/index.php/APST/index

Published by the Research and Graduate Studies,
Khon Kaen University, Thailand

A fatigue and stress distribution analysis of horizontal axis wind turbine blade

Fakada D. Gurmesa[1], Johnson A. Santhosh[1,*], Biniyam A. Abebe[2], Demeke G. Waskhume[1] Firew T. Kassaye[1] and Yahiya A. Kedir[1]

[1]Faculty of Mechanical Engineering, Jimma Institute of Technology, Jimma University, Jimma, Ethiopia
[2]Department of Mechanical Engineering, College of Engineering & Technology, Wolkite University, Ethiopia
[*]Corresponding author: johnsonsanthosh@gmail.com

Received 6 October 2020
Revised 22 February 2021
Accepted 25 February 2021

Abstract

Fatigue stress distributions developed on the wind turbine lead to fatigue failure due to various loads. The present study was performed under various loads such as gravitational load, centrifugal forces, and aerodynamic forces (lift and drag pressure) for Horizontal-Axis Wind Turbine (HAWT) blade made of composite materials (E-glass fibre). Fatigue failure analysis of wind turbine blade type the National Advisory Committee for Aeronautics (NACA) 4412 performed under wind speed of 35 m/s. After completing both the Computational Fluid Dynamics (CFD) and static structural analysis, the output results such as total stress, deformation, and shear stress are identified. Simultaneously, critical locations on the blade are shown on the CFD results. It is concluded that the maximum stress location in a wind turbine is the blade's leading edge and the blade root (part the nearer of the hub). The wind speed increases beyond recommendation design, and it decreases the life of the wind turbine blade. The blade's leading edge is more deformed, and the centrifugal load is considered the most influential factor in the life of the blades.

Keywords: Horizontal Axis Wind Turbine, Composite Wind Turbine Blade, Computational Fluid Dynamics, Fatigue life, Fatigue Analysis, Wind Energy

1. Introduction

Currently, the utilization of renewable energy sources is the primary international attention to overcome global warming. Wind energy generated from wind flow by the wind turbine is one of the available renewable energy with significant potential. Nowadays, investment from developed countries is to develop renewable energy systems, and one of the important demanded at the site of high wind flow speed is wind energy [1,2]. This study deals with fatigue problems and stress distribution of the Horizontal Axis Wind Turbine (HAWT) blades, which produce electric power from wind flow velocity pressure. One of the critical issues in a wind turbine is the downtimes due to the blades fatigue failure [3,4].

The cause of the fatigue on the blade and fatigue load can be fundamental, which means the actual load applied on the blade. The specific load reaches the limit state, and the question may become a load beyond its permissible value. The blade can be broken down during loading and unloading events, or it may cause resonant stresses on the blade [5,6]. The result of the study observed on HAWT blade made of composite material is that the causes of fatigue analysis on the blade are turbine operating speed, environmental effect, operating condition (braking and idling), and geometry of the blade [7]. The causes of fatigue failure of the wind turbine blade are environmental conditions; cyclic load decreases the stiffness of the materials, which leads to crack initiation and minimizes the service life of the blade's structure [8] and which does not specify the factors in the environment. The fatigue damage is because of the blade under different wind loads and applying the Reliability-Based Design Optimization (RBDO) technique to a safe blade of the wind turbine as well as economical designs considering [9]. There are plenty of investigations on the fatigue damage accumulation area on the wind turbine blade and identify where stress is maximum on the blade. Accordingly, parameters that govern the interface elements' properties and clarify that the blade's length is inversely proportional to blade fatigue life [10,11]. The

primary fatigue damage is on the surface, and edge damage, fibre failure, fibre/matrix deboning, matrix cracking, and delamination, which are dependent on the orientation of the fibres initiated from the surface, and edge damage then goes global body [12]. In contrast, other investigations suggest that the blade's residual strength and the rotational operation of blade delamination of the inner layer lead to failure at blade root and the higher stress concentration is near the root blade [13,14].

Among fatigue analysis methods, the investigation from three different crack propagation models is; the linear Miner model, Paris model, and Reifsnider model, which give more reliable results to simulate composite blades crack growth under practical situations [15]. According to Castro et al. [16], the studied result, the accumulation damage, and the stress spectra on the layer are calculated using laminated composite theory and rain-flow cycle counting method, which was, implemented to analyze the uniaxial stress series. Samborsky et al. [17] investigate the result, which indicates that the ductility materials due to the adhesive composition of the composite or the environment's conditions may change this behaviour, and FEA is used to identify the local stress concentrations and pore locations. The other studied results show that stochastic fatigue models give reliable results and are used for analyzing the failure probabilities of the composite blades [18,19]. In the assessment of fatigue resistance materials for wind turbine design blades, a Uni-Directional (UD) laminate and a Triax laminate are used to increase the strength in theoretical calculations and experimental results [20].

According to Kulkarni et al, [11] and Maldhure [21] study, if the approximate cost of a woodwind turbine blade is given for every five years of reliability; when it compares to the composite material, each blade is tripled to wood cost for 15 years of reliability. It means costs for blade material and downtime due to failure of the blade are avoided.

Even though many literature outputs on the fatigue failure analysis of wind turbine blades are analyzed and discussed in the previous section, gaps hinder various load stress results on the blade for each load. The literature study results focus on the blade parameters, void content in the blade materials, and the composite materials interlamination. Some researchers investigate aluminium material for the causes of fatigue, fatigue analysis methods, and fatigue resistance materials. However, many researchers do not identify which load is highly affecting the wind turbine blade, and the reason why that load affects the blade is not addressed. Their result observations do not suggest which load has more effect on the leading edge of the blade stressed/affected. No information is identified about the thickness of the blade, frame (web) material, and its thickness, the number of plies (layer) on composite materials. The fibre orientation was neglected in some of the observed results. In this study, the loads with their stress result with all information composite and blade parameters are included. The gap that is not studied in depth is addressed using static structural and Computational Fluid Dynamics (CFD) Modules in ANSYS software package.

2. Materials and methods

The methodology of this study is illustrated in Figure 1. For fatigue analysis and stress distribution of HAWT blade, the study design is divided into two parts, namely;

i. Calculation of blade parameters and 3-D model of the blade by Computer Aided Three-dimensional Interactive Application (CATIA)
ii. CFD and Finite Element Analysis (FEA) modelling

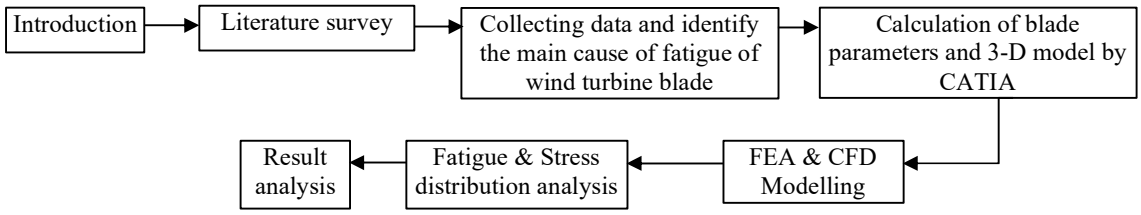

Figure 1 Flow chart for blade analysis procedure.

2.1 Calculation of blade parameters and 3-D model by CATIA

The airfoils used in this wind turbine blade are the aviation airfoils under the National Advisory Committee for Aeronautics (NACA) series [22]. Blade parameters used to maximize the blade efficiency and optimize wind turbine performance are essential for a 3-D model, such as twisting angle, tip speed ratio, chord length, blade setting angle, and lift & drag coefficient. Twist angle of the blade and variables of the angle of attack through the length of the blade are specified. This twist angle is vary based on the drag and lift coefficient ratio $(C_D)/C_L)$ and each individual parameters of the airfoil at specified angle of attack [18]. The angle of attack is translated to the angle of relative wind by adding the initial twist angle of the blade.

$$\phi = \frac{2}{3} tan^{-1}\left(\frac{1}{\lambda_r}\right) \quad (1)$$

where: λ_r is the local speed ratio, $\lambda_r = \frac{\lambda_D \, r}{L_b}$; λ_D is design tip speed ratio which is read from the figure of blade number and design tip speed ratio, r is the length of the blade at an instant, L_b is the total length of blade. In this study, design tip speed (λ_D) ratio taken is 5. The chord length (c) distributed on each airfoil through blade length also varies with the as mentioned in equation (2) as

$$c = \left(\frac{8\pi r}{BC_{LD}}\right)(1 - cos\phi) \quad (2)$$

where: B is blade number and C_{LD} is the lift coefficient of airfoil design.
After these parameters are known, the design procedure involves determining the chord length c and blade setting angle β at various lengths of the aerofoil. The lift coefficient (C_L) at various sections can be calculated by

$$C_L = \frac{(8\pi r)}{B\,c}\left\{1 - \cos\left(\frac{2}{3}\tan^{-}\left(\frac{L_b}{\lambda_D\, r}\right)\right)\right\} \quad (3)$$

Angle of attack, $$\alpha = A_1 + A_2 C_L - A_3 C_L^2 + A_4 C_L^3 \quad (4)$$

where: Constants, $$A_1 = 6.5; \quad A_2 = -25.0; \quad A_3 = 21.0; \quad A_4 = -1.0$$

The angle of blade setting, β of blade partitions at r distance from the aerofoil centre can be determined by using sets of relationships as

Blade setting angle, $$\beta = \phi - \alpha \quad (5)$$

Area of each blade, $$A_b = c_{avg} \times L_b \quad (6)$$

where: c_{avg} is average chord length and L_b is the length of blade.

Swept area, $$A_s = \frac{\pi}{4} D^2 = \pi L_b^2 \quad (7)$$

Solidity, $$\sigma = \frac{BA_b}{\pi L_b^2} \quad (8)$$

Total blade area, $$A_T = \sigma \times A_s = B \times c_{avg} \times L_b \quad (9)$$

Airfoil thickness, $$t_a = 0.12 \times \text{chord length} = 0.12 \times c \quad (10)$$

Table 1 Assumptions of turbine blade specifications.

No.	Specification
1	Airfoil Type: NACA4412
2	Blade length, L_b:1220 mm
3	Configuration: 3 blades
4	Number of layers: 5
5	Lamina thickness, l_t: 1 mm
6	Fibre orientation: $[\pm 45^{\circ}, 0^{\circ}]$
7	Rotational speed: 17 rpm
8	Hub diameter, D: 120 mm
9	Speed of Wind v: 35 m/s
10	Density of air, ρ_a: 1.225 kg/m^3
11	Laminate thickness, t: 5 mm

Turbine blade specifications are assumed to carry out fatigue stress distributions analysis. Assumptions of Turbine Blade Specifications are shown in Table 1. Fibre orientation in each layer of the structure is arranged in an order such as five plies (layers) with each of $45^{\circ}, -45^{\circ}, 0^{\circ}, -45^{\circ}, 45^{\circ}$ with 1mm of each ply's thickness, 5 mm thickness of the blade made of E-glass fibre. One angle is used for making one ply (layer). Thus, using five

angles with 1 mm ply thickness, the blade thickness (E-glass fibre) is 5 mm. In the design, the available performance of data of NACA4412 aerofoil, the minimum of C_D/C_L is of 0.01 with 4° of an angle of attack and the corresponding C_{LD} value is 0.8.

In this study, NACA 4412 four-digit code airfoil is used to describe the airfoil shapes. The 1st digit indicates the maximum camber of chord in percentage and the 2nd digit indicates the location of maximum camber from leading-edge alongside chord line in tenths of the chord. Lastly, the 3rd and 4th digits indicate the percentage of the chord of the maximum thickness.

The blade is divided into fifteen sections with airfoils separated by a distance of 70 mm, as shown in Table 2. All parameters determined are used to set the airfoil shape with the order of position to draw a 3-D model of the blade. The division is to obtain the actual profile shape of the blade. This sectional division can be other numbers (more or less than fifteen) of sections. Fifteen sections are perfectly fitted to set the airfoil shape in this study. Section 1 is the root chord, and its length is 239 mm, and section 15th is the tip whose length of the chord is 94 mm long. The length of the hub is 80 mm, the hub to blade neck is 90 mm, and the length through chord is 1050 mm.

Table 2 Distribution of calculated blade parameters.

Section	Sectional radius (m)	Twist angle ϕ (degree)	Local speed ratio λ_r	Chord length, c (m)	Airfoil thickness, t_a(m)	Blade setting angle, β(degree)
1	0.070	47.7	0.333	0.240	0.0288	43.7
2	0.420	37.5	0.667	0.302	0.0364	33.5
3	0.210	30.0	1.000	0.294	0.0354	26.0
4	0.280	24.6	1.333	0.268	0.0322	20.6
5	0.350	20.6	1.667	0.234	0.0281	16.6
6	0.420	17.7	2.000	0.208	0.0249	13.7
7	0.490	15.5	2.333	0.186	0.0223	11.5
8	0.560	13.7	2.667	0.167	0.0200	9.7
9	0.630	12.3	3.000	0.151	0.0182	8.3
10	0.700	11.1	3.333	0.137	0.0165	7.1
11	0.770	10.2	3.667	0.127	0.0153	6.2
12	0.840	9.4	4.000	0.118	0.0142	5.4
13	0.910	8.7	4.333	0.109	0.0132	4.7
14	0.980	8.0	4.667	0.100	0.0120	4.0
15	1.05	7.5	5.000	0.094	0.0114	3.5

The blade length is considered as the summation of these three parts i.e. 80 mm + 90 mm + 1050 mm = 1220 mm. The blade, divided into fifteen sections and shown in Table 2, has the length of the frame (web) 1080 mm, which is the 13th airfoil at the tip of the blade.

To draw a 3-D model blade with NACA 4412 airfoil number, the procedure shown in Figure 2 was performed in CATIA V5R19 Modeling software.

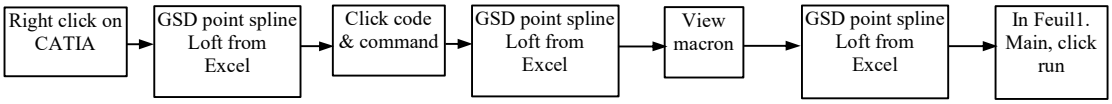

Figure 2 Blade model procedure in CATIA.

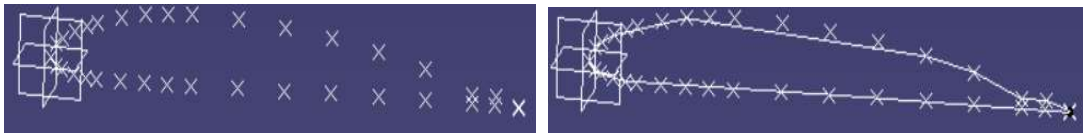

Figure 3 Points and splines generated from NACA 4412 airfoil number.

Once the spline of the airfoil profile of NACA 4412 is generated, as shown in Figure 3, the result calculated and presented in Table 2 is used to draw the 3-D Model of the blade to get the desired chord length (C), airfoil thickness (t_a), twisting angle, and blade setting angle (β) of the blade. After cleaning the points on the spline and correct smoothness of the spline line, using a scale, offset and copy-paste the spline airfoil shape at distant needed (70 mm apart for 15 times) until the length of the blade with its dimension is performed. The blade of a 3-D model on Figure 4 (B) is drawn with the arranged airfoils as indicated in Figure 4 (A) is made of E-glass fibre and frame (web), which is used to make more stiff the blade is made of aluminium alloy.

The frame (web) is modelled from a 3-D drawing by scale (reducing dimension) in three coordinate systems and cut out, as shown in Figure 4 (C). The wind turbine blade assembly with their frames is shown in Figure 5 (A) and (B), respectively.

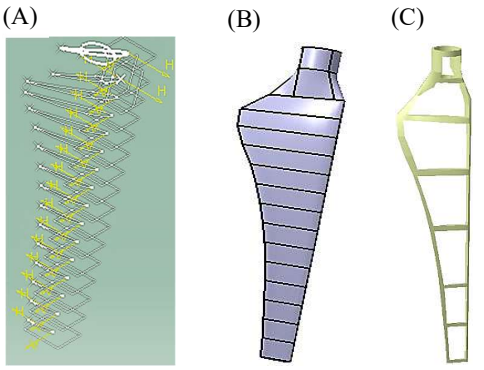

Figure 4 (A) Arrangement of airfoils, (B) 3-D model of the blade, and (C) Frame (Web) of blade.

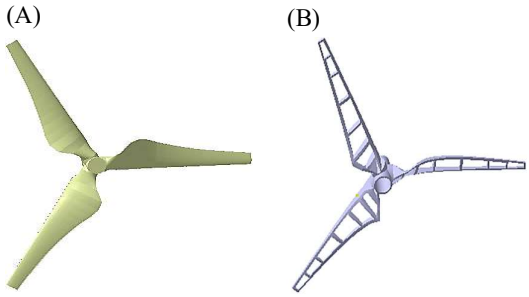

Figure 5 (A) Blade made of the E-glass fibre and (B) Frame (web) made of aluminium alloy.

The critical parameters of wind turbine blades are calculated using the following expressions.

$$\text{Wind speed pressure, } P = \frac{1}{2}\rho_a V_{ult}^2 \tag{11}$$

where, V_{ult} is ultimate wind speed and ρ_a air density

$$\text{Lift Force, } F_L = \frac{1}{2}\rho_a V_{ult}^2 A_b C_L \tag{12}$$

$$\text{Drag Force, } F_D = \frac{1}{2}\rho_a V_{ult}^2 A_b C_D \tag{13}$$

where, C_L and C_D are the coefficient of lift and drag, respectively.

$$\text{Lift pressure, } \quad P_L = \frac{F_L}{A_b} \tag{14}$$

$$\text{Drag pressure, } \quad P_D = \frac{F_D}{A_b} \tag{15}$$

$$\text{Resultant pressure, } P_R = (P_L^2 + P_D^2)^{1/2} \tag{16}$$

The force experienced by the rotor, which is known as thrust force (F_T) expressed as:

$$F_T = \frac{1}{2}\rho_a A_T V^2 \tag{17}$$

The rotor torque (T) is defined as

$$T = F_T R = \frac{1}{2}\rho_a A_T V^2 L_b \quad (18)$$

$$\text{Centrifugal Force, } F_C = m_b \omega^2 L_b \quad (19)$$

where, m_b is the mass of the blade, and ω is the rotational velocity of the blade.

$$\text{Gravitational load, } F_g = m_b g \quad (20)$$

where: g is the gravity acceleration.

Consider blade rotate without any resistance and use wind speed as tangential speed,

$$\text{Tangential speed, } V_t = r\omega = L_b \omega \quad (21)$$

where: r represents the length of the blade at instant and ω represents rotational blade speed.

The wind turbine blade's critical parameters are calculated using the above formulas, and the results with the corresponding values of variables are given in Table 3.

Table 3 Parameters numerical calculation results of the wind turbine blade.

Parameters	Formula	Values	Result
Area of the blade, A_b	Equation (6)	$c_{avg} = 0.1823$ m, $L_b = 1.22$ m	0.2224 m^2
Swept area, A_s	Equation (7)	$L_b = 1.22$ m	3.83 m^2
Solidity, σ	Equation (6-8)	B = 3, $c_{avg} = 0.1823$ m, $L_b = 1.22$ m	14.27%
The total area of the blades, A_T	Equation (6-9)	$\sigma = 0.1427$, $A_s = 3.83$ m^2	0.5465 m^2
Maximum airfoil thickness, t_{max}	Equation (2,10)	$c_{max} = 0.302$ m	36.24 mm
Minimum airfoil thickness, t_{min}	Equation (2, 10)	$c_{min} = 0.094$ m	11.28 mm
Wind speed pressure, P	Equation (11)	$\rho_a = 1.225$ kg/m^3, $V_{ult} = 35$ m/s	750 Pa
Lift force, F_L	Equation (6,11-12)	$\rho_a = 1.225$ kg/m^3, C_L = 0.8, A_b = 0.2224 m^2, $V_{ult} = 35$ m/s	133 N
Drag force, F_D	Equation (6,11,13)	$\rho_a = 1.225$ kg/m^3, C_D = 0.008, A_b = 0.2224 m^2, $V_{ult} = 35$ m/s	1.335 N
Lift pressure, P_L	Equation (6,12,14)	$F_L = 133$ N, $A_b = 0.2224$ m^2	600 Pa
Drag pressure, P_D	Equation (6, 13,15)	$F_D = 1.335$ N, $A_b = 0.2224$ m^2	6 Pa
Resultant pressure, P_R	Equation (14, 15-16)	$F_L = 600$ N, $F_D = 6$ N	600 Pa
Torque, T	Equation (19)	$A_T = 05742$ m^2, $V_{ult} = 35$ m/s	452 Nm
Centrifugal force, F_C	Equation (20)	$\rho_a = 1.225$ kg/m^3, $L_b = 1.22$ m $m_b = 1.25$ kg, $\omega = 28.68\ rad/s$, L_b=1.22 m	1.25 KN
Gravitational load, F_g	Equation (21)	$m_b = 1.25$ kg, g = 9.81m/s^2	12.262 N
Rotational speed of the blade, ω	Equation (22)	V_t= 35 m/s, L_b=1.22 m	28.69 Rad/s

2.2 CFD and Finite Element Method (FEM) modeling

2.2.1 CFD modelling

CFD provides many advantages compared with experimental fluid dynamics, such as lead time in design and development is significantly reduced; can simulate flow conditions without reproducible in the experimental model test; provides more detailed and comprehensive information; is increasingly more cost-effective than wind tunnel testing and produces lower energy consumption [23-25]. The work is analyzed with the importance of the governing equations of CFD. The continuity equation for the three-dimensional steady flow is:

$$\nabla.(\rho V) = \frac{\partial(\rho u)}{\partial x} + \frac{\partial(\rho v)}{\partial y} + \frac{\partial(\rho w)}{\partial z} = 0 \quad (22)$$

For viscous flow in the x-direction, the momentum equation is:

$$\rho \frac{Du}{Dt} = \frac{\partial \rho}{\partial x} + \frac{\partial \tau_{xx}}{\partial x} + \frac{\partial \tau_{yx}}{\partial y} + \frac{\partial \tau_{zx}}{\partial z} + \rho \int x \quad (23)$$

Reynolds-averaged Navier-Stokes (RANS) equation is defined as:

$$\rho \frac{DU_i}{D_t} = \frac{\partial P}{\partial X_i} + \frac{\partial}{\partial X_i}\left[\mu\left(\frac{\partial U_i}{\partial x_i} + \frac{\partial U_i}{\partial x_i}\right) - \rho\overline{\bar{u}_i \bar{u}_j}\right] \quad (24)$$

The change in mean momentum of the fluid element and the mean body force average stress represent the left-hand and right-hand sides of the equation. While an unknown term is called Reynolds stress $\rho\overline{\bar{u}_i \bar{u}_j}$. Smagorinsky - Lilly: Smagorinsky develops the eddy-viscosity as:

$$\mu_t = \rho L_s^2 |\bar{S}| \quad (25)$$

where L_s is the mixing length for scales of subgrid and $|S| = \sqrt{2\bar{S}_{ij}\bar{S}_{ij}}$ $\bar{S}_{ij}$ is the resolved scale which is the rate-of-strain tensor defined by $\bar{S}_{ij} = \frac{1}{2}\left(\frac{\partial \bar{u}_i}{\partial \bar{x}_j} + \frac{\partial \bar{u}_j}{\partial \bar{x}_i}\right)$ and $L_s$can be computed using:

$$L_s = \min(\kappa d, C_s \Delta). \quad (26)$$

where κ is the von Karman constant ≈ 0.41, d is the distance to the closest wall, C_s is the Smagorinsky constant, and Δ is the local grid-scale based on the element volume. C_s = 0.23 for homogenous isotropic turbulence in the inertial subrange is derived a value by Lilly. The three main elements, CFD Package are pre-processor, solver, and post-processor. In this study, the blade is treated in the stationary wall condition with the no-slip shear condition, and wind speed is taken, which is considered at maximum as shown in Table 4, the tangential speed, $V_t = 35$m/s, which can calculate from the formula of

$$V_t = r\omega = L_b\omega \quad (27)$$

where: r represents the length of the blade at instant, L_b represents total blade length and ω represents the rotational speed of the blade. For this study, the average pressure at sea level is 1013.25 mill bars taken from Adama Wind Farm, Ethiopia.

Table 4 CFD parameters input.

Parameter	Value
Airfoil types	NACA 4412
Fluid Material	Air
Temperature, T	295 K
Air density, ρ_a	1.225 kg/m^3
Kinematic Viscosity, η	1.470 ×10^{-5} m^2/s
Reynolds Number, R_e	1×10^5
Pressure, P	10.13 KPa
Wind Speed, V_t (maximum)	35 m/s
Rotor diameter, D	2.44 m

CFD analysis investigates the wind flow pressure distribution and the effect on the wind turbine blade, which has been performed in the ANSYS FLUENT module. The study was conducted with a blade length of about 1.22 m by exposing the assembled three blades to wind at a high speed of 35 m/s, which is significantly higher than most wind turbine operations. When the wind speed becomes very high, the turbine is locked with pitch control, and the blade are stopped.

In this CFD analysis, the material properties are not important because the simulation result indicates only the aerodynamic (wind speed) distribution effects on the blades and the critical section/ area the pressure of wind speed affects the wind turbine blade. Thus, in the case of material property, using default material has no result change. The software to compute and indicate the wireframe meshed structure and frame mesh on the surface, as shown in Figure 6 (A) and (C), uses the Finite Volume Method (FVM).

The 3-D model blade assembled was imported into a computational fluid domain. Figure 6 (A), which has a complete circular inside it and the entire circle domain, covers the blades as depicted in Figure 6 (C). The computational domain size is enclosed in a rectangular box with dimensions x =5 m, y = 4 m, and z = 6 m. The simulation 3-D models performed under box volume. The circular part at which wind speed section is bounded

in the air box. The volume cell at which the simulation blade is inside the circular domain with a 3 m and 2 m depth diameter. The simulation results of the aerodynamic effect on the blade are observed from the CFD post, processed in the ANSYS Fluent. 3-D Assembly model from CATIA V5R19 is imported into ANSYS Fluent. The blade is considered a free rotating body. The Finite Volume Method (FVM) details of the implementation are on unstructured meshes or taken only space bounded. The performance of the blade does not predict using CFD predetermined aerodynamic data. Instead, the governing equations of fluid in all direction on the surface blade is computed in an iterative process by CFD solver. Such a technique leads to blade span wind speed analysis on the blade and the fluid interaction effects, including friction losses 3-D body.

In this study, the only inlet flows wind speed is specified as the inlet boundary type. Figure 6 (A) shows that the stationary air domain where the environment is considered as the wind speed pushes the wind turbine blade. Gravity has a periodic variation in the process of blade rotation and has a significant influence on the edgewise moment [26]. The gravitational load is the vertical forces acting on the structure. In CFD analysis using ANSYS Fluent, the wind speed is treated as equal to 35 m/s. The simulation result shows the aerodynamic effect distributed on the blade's surface and pressure acting on the blade during the wind turbine operation. Figure 7 indicates that gravitational load affects the leading edge of the blade and the aerodynamic effect has a significant impact on the tip of the blade, especially the leading edge.

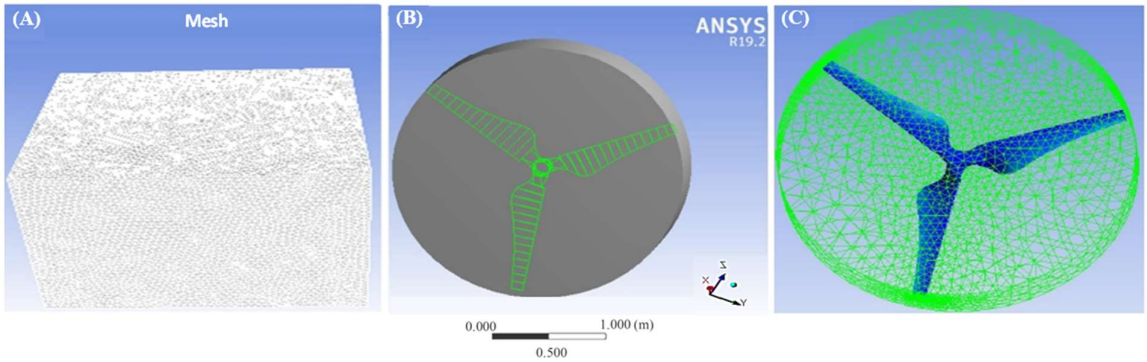

Figure 6 (A) Wall stationary air domain box mesh, (B) The blades inscribed in circular rotation domain, and (C) Circular bounding blade region with mesh.

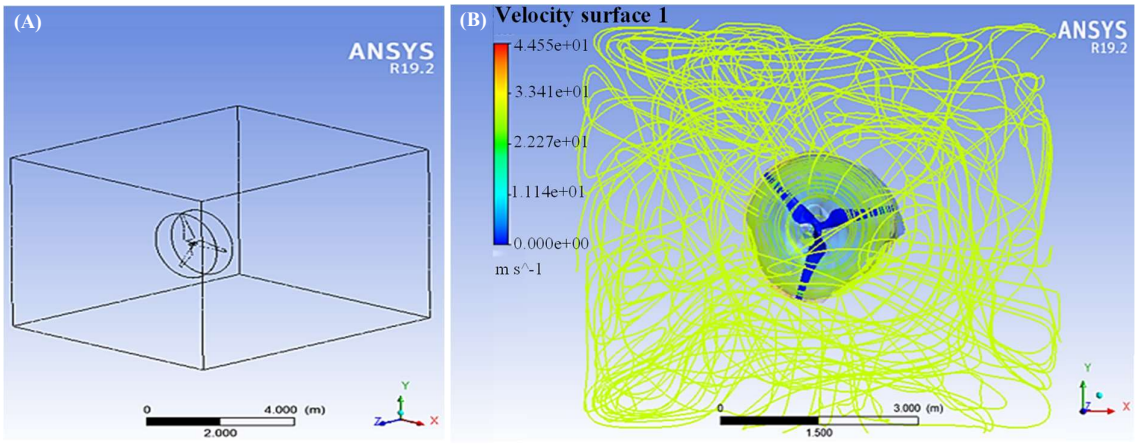

Figure 7 (A) Blades enterer circular domain in the outer wall box and (B) Wind velocity streamline during the blade rotation.

Figure 7 (B) Demonstrates the rotating blade. During the wind turbine blade operation, wind stream flows make the turbulence of wind flow, as demonstrated in Figure 7 (B). It makes the non-linear bending stress on the blade redundantly, which leads the blade to fatigue failure. Figure 8 is taken from the convergence graph of CFD solution. The error in the solutions and the local imbalance of the conserved variable determines the convergence of iterative solutions. Solutions are directly quantified in scaled residual value for each control volume. The Viscosity from Figure 8 was changed as indicated on the legend, and the value was high at the red colour, more specifically around the tip of the leading edge of the blade. It goes increasingly from the centre to the blade tip, and the tip of the leading edge of the blade is highly pressurized, which may make the blade to be deformed. These leading-edge surfaces gradually can have eroded by wind flow which leads to fatigue failure.

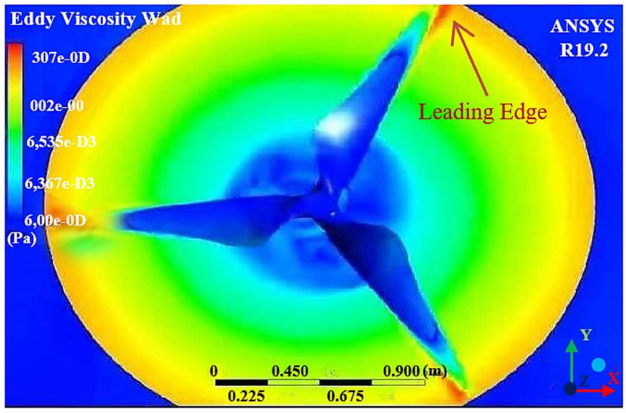

Figure 8 Eddy viscosity effect on the blade during operation and affected leading edge.

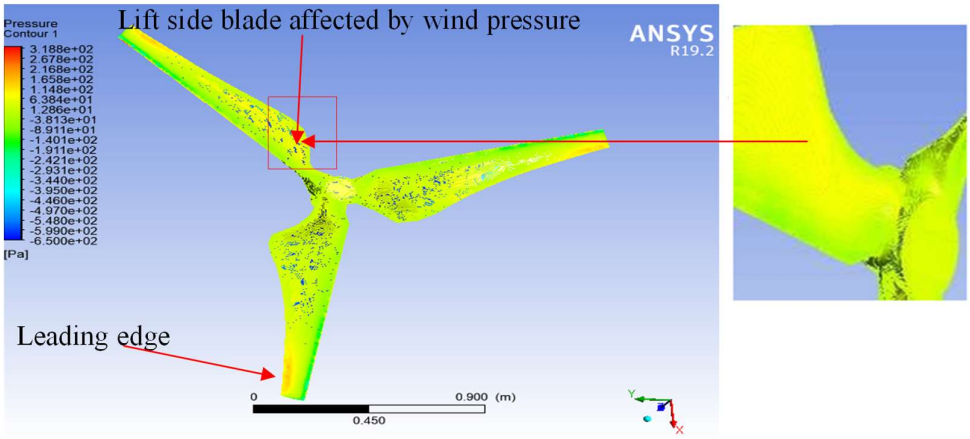

Figure 9 Aerodynamic pressure effect on the wind turbine blade.

Figure 9 shows that the leading edge and the blade body near the hub where pressure is highly loaded and the air velocity drop on the side of the blade's trailing edge due to the rotating blade's wake formation. The pressure contour shows a high-pressure spot on the leading edge. It indicates the pressure imbalance on the tip and the hub centre. The tower height is a mandatory input for high wind pressure. Because the blade is highly affected by lift and drag pressure (aerodynamic effect). Tower height increases for various loads act on wind turbine blades except gravitational load. As demonstrated in Figure 10, the blade on the drag position wind pressure side is low. As shown in Table 2, the analytically calculated drag pressure is 6 N depending on blade parameters.

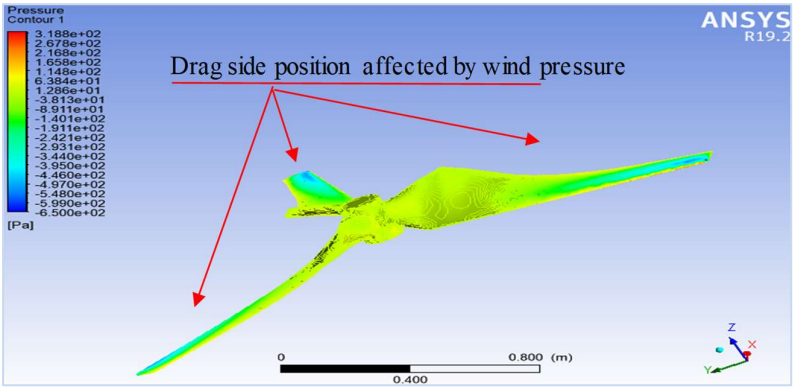

Figure 10 Wind pressure effect on the side of the drag position of the blade.

The velocity vector field around the skin of the blade and pressure contours were obtained as shown in Figure 11. Figure 11 (A) Shows the incremental velocity distribution effect with increasing the blade length and

field of velocity vector on the surface skin of the blade. The red side of the spectrum shows that the value of the velocity is relatively high. The velocity of the blade increased from the root to tip. Notably, the axial velocity increased at a uniform pattern with the increasing length of the blade. These phenomena justify that blades perform high centrifugal force with incremental length.

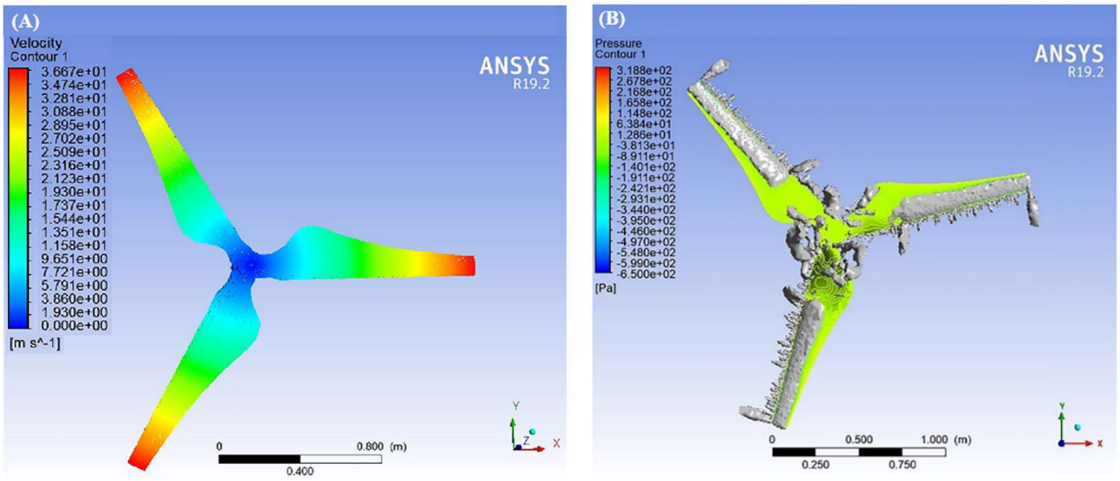

Figure 11 (A) Velocity distribution on blades and (B) Vortex core region on the blades.

Figure 11 (A) shows a pressure difference between roots and the tips of prevails that wind speed increased with the wind turbine blade's length. Consequently, the stressed area is increased with the incremental velocity of the wind. In the vortex core region shown in Figure 11 (B), the pressure-flow from high value to the low region demonstrates that the high pressure from lift side to drag side make turbulence wind flow.

Generally, in the Computational Fluid Dynamics (CFD) simulation result, the blade's aerodynamic effect shows the similarity of wind pressure with the wind flow's actual distribution. These all of the above Computational Fluid Dynamics (CFD) simulation results are used to achieve specific objectives such as aerodynamic effect, stress distribution, and the critical area where stress is maximum on the blade.

2.2.2 FEM modelling and static structure analysis

The Material properties of aluminium alloy are used for the web (frame) of the blade. The composite property is calculated analytically from the mixed materials (fibre and resin) using the mixture rule formulas. The result is presented in Table 5.

Table 5 Material properties for wind turbine blade.

E-glass fibre UD > Orthotropic elasticity								
Young's Modulus X, MPa	Young's Modulus Y, MPa	Young's Modulus Z, MPa	Poisson's Ratio XY	Poisson's Ratio YZ	Poisson's Ratio XZ	Shear Modulus XY MPa	Shear Modulus YZ MPa	Shear Modulus XZ MPa
45,852	13,400	13,400	0.1952	0.2287	0.1952	5,516	5,453	5,516
E-glass fibre UD > Orthotropic stress limits								
Tensile in X MPa	Tensile in Y MPa	Tensile in Z MPa	Compressive in X MPa	Compressive in Y MPa	Compressive in Z MPa	Shear XY MPa	Shear YZ MPa	Shear XZ MPa
253.36	16108	16,108	-28,245	-9150	-1150	850	180	850
Properties of aluminium alloy which used for web (frame) of the blade								
Density		Compressive Yield Strength MPa		Tensile yield strength, MPa		Tensile ultimate strength, MPa		
2.77e-006 kg/mm^3		280		280		310		

The 3-D drawing is modelled depending on the parameters, with its result given in Table 2. The highly pressurized part in the Computational Fluid Dynamics (CFD) result on the blade is again analyzed in static structural considering the material properties. The result is analogous in the case of stress distribution location. In this study, to perform a FEM simulation in the ANSYS 19.2 software, the following steps are considered:

1) Specification of the material properties collected for the following cases,
- Aluminium alloy material properties for the frame (web) of the blade
- E-glass fibre material properties for the outer body of the blade

2) The following steps are implemented in ANSYS using the material properties,
- First, ACP (Pre) tool in ANSYS is selected to build surface layers under ACP-Pre model tree E-glass fibre

property is activated and with five number of plies, 1 mm thickness for each ply, fibre orientations [±45°, 0°] up to Modeling Groups then at last update scene 1.

- From ANSYS Toolbox, Static Structural is picked out, then set up from ACP-Pre is joined with Model in theStatic structural. Gravitational load, the rotational speed of the blade, lift and drag forces which are determined, and presented in Table 2 applied as their directions and,
- With loads, total deformation, maximum and minimum deformation, equivalent stress, shear stress, maximum stress are simulated with ANSYS 19.2

In this study, the boundary conditions depend on the fatigue and stress cause blades of the wind turbine. The blade is supposed a cantilever beam subjected to uniaxial (gravitational) and multi-axial loading (both drag and lift forces) conditions that make the deformation. The blade is fixed support at the hub, which resists moment force like a cantilever beam on only one end. The bending moment with equivalent point (gravitational load/weight of the blades) and uniformly distributed loads (aerodynamic loads) act on the blades similar to the cantilever beam. The fixed (rigidly) mounted blades on the hub were made the same way as the cantilever beam.

Theoretically, a wind turbine blade is considered free rotating, and boundary conditions point out as no constraint in a mechanism model, which is typically a good approximation. However, in practice, the free boundary condition does not carry out on the blade's root. A fixed boundary condition works on the root, but modelling this boundary condition as completely rigid introduces uncertainty as it is not fixed. The finite element method is used to complete the fatigue analysis, as previously mentioned.

Full wind load (pressure) is applied as usual to the blade on both sides as lift and drag force without any loss. There is a numerical calculation in Table 2 using finite element analyses to estimate the life span of the blade to complete the analysis. This boundary condition is applied as a cantilever beam type. The beam root was fixed rigidly with 6 Degrees of Freedom (DOF). Among the wind force on the wind turbine blade, only the normal pressure, both lift and drag force, should be considered. The gravitational load is towards the earth, and rotational speed is applied in the z-axis with a clockwise direction. Generally, the loads applied to analysis fatigue failure are gravitational load, the blade's rotational speed, lift and drag forces. The result for the desired analysis has been explained using boundary conditions in the following section.

2.2.3 Static structural analysis result

First, the blade is modelled by surface extrude with 0 thickness. After importing the model to ANSYS with the material properties (E-glass fibre), the thickness and fibre orientation are written in ACP- (Pre) module. The blade model of composite material with a thickness of 5 mm is generated. The total deformation in Figure 12 (A) shows contour along the blade span due to all applied loads considered in this study. The total deformation of 5.1964 mm was found at the tip of the blade. This due to the blade is treated as a cantilever beam, and as the length of the beam far from the fixed joint, the deflection has become high. As shown in Figure 12 (B), the maximum Von-Mises stress is 40.891 MPa, and the minimum Von-Mises stress is 0 Pa with loads (gravitational load, centrifugal load, lift and drag pressure).

From this simulation stress analysis of the blade, maximum stress is generated around the root of the blade. Figure 12 (C) demonstrates that the maximum principal stress is 46.996 MPa with loads (gravitational load, centrifugal load, lift, and drag pressure). The simulation of this stress analysis result on the blade shows that maximum stress generated found at the site similar to equivalent stress around the blade's root. Figure 12 (D) shows that the minimum principal stress on the blade. It indicates that normal stress is calculated at an angle, and in this case, shear stress is treated as zero and its maximum value 8.1245 MPa while the minimum value is -32.945 MPa. This negative sign shows stresses are compressive. Figure 12 (E) shows the safety factor is 4.9998 $\approx$ 5, which implies the wind turbine blade will account for five times the expected force (5 times as strong as the applied loads or the stress). Therefore, the wind turbine blade is safe for the applied loads. Figure 12 (F) shows the fatigue damage of the wind turbine blade. Fatigue damage development in composite materials is unlike in metals that follows damage accumulation, including matrix cracking, fibre fracture, debonding, transverse ply cracking, and delamination. In this analysis, the thickness and number ply in the blade's composite might not increase the strength. But the damaged area has analogous to other thicknesses and any loads applied to the blade shape.

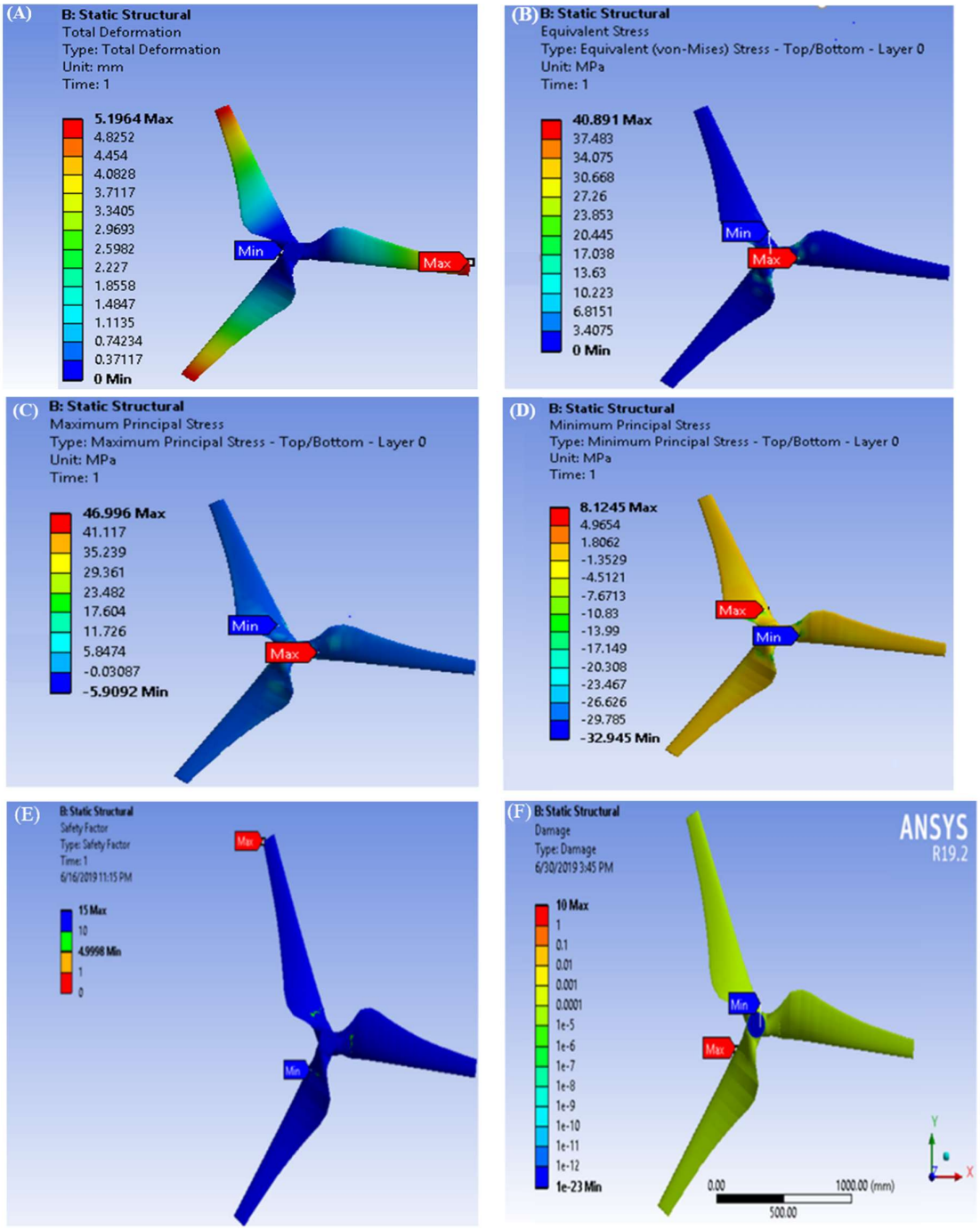

Figure 12 (A) Total deformation of the wind turbine blade, (B) Equivalent (Von-Mises) stress of wind turbine blade, (C) Maximum principal stress of the HAWT blade, (D) Minimum principal stress on the blade, (E) Safety factor of the blade and (F) Damage simulation of the wind turbine blade.

3. Results and discussion

Table 6 shows that the maximum simulation result obtained shows that the critical area at which the blade becomes fail through gradual, which is called fatigue failure. From each load, the minimum and maximum stress are calculated by drag and centrifugal load, respectively. The stress values are lower than the yield strength of the material in E-glass fibre, which is desirable. Fatigue failure occurs because of crack growth reaching critical size, resulting from cyclic loads on the blade. Due to bending stress, there is tensile stress in the trailing edge

and compression in the leading edge, and again, the shear stress has induced. These tensile and compression stress are performed repeatedly and changeably with wind speed. According to the results of these all analyses, the maximum stress is generated on the blade root under extreme loads, and it is caused by centrifugal. The maximum stress greater than this centrifugal load is when total loads are applied at once.

Table 6 The result ANSYS simulation by different types of loads.

Load Type	Drag pressure	Gravitational load	Lift pressure	Centrifugal load	Lift and drag pressure, gravitational and centrifugal load at once
Total deformation	0.020 mm	0.679 mm	2.021 mm	3.864 mm	5.196 mm
Elastic strain, τ_{max}	4.97e-6	14.30e-6	4.8e-4	1.71e-3	2.05e-3
Von-Mises stress	0.103 MPa	3.405 MPa	10.167 MPa	34.414 MPa	40.891 MPa
Max. principal stress	0.082 MPa	0.479MPa	11.739 MPa	39.491 MPa	46.996 MPa
Max. shear stress	0.056 MPa	1.86 MPa	5.549 MPa	18.9 MPa	22.456 MPa

Life Analysis of Blade of Wind Turbine is shown in Figure 13, and the fatigue life of a blade of the wind turbine is approximated. The analysis is performed on a blade made of composite material (E-glass fibre) thickness of 5 mm for the outer shell part and 3mm aluminium for the frame (web). The blade of wind turbine parameters that govern fatigue life are the length of the chord, length of the blade, and angle of twist. Fatigue life is the total number of load cycles that the material or structure can endure before failure. Note that the 3-D engineering model of a blade of the wind turbine in this study can operate for a minimum of 11.2 years, depending on the result in Figure 18, which means that a machine operating at 17 rpm exposed to Year x 365 x 24 x 60 x 17 rpm = 108 stress cycles. (Life = 11.2 years). It implies the typical model analysis of the wind turbine blade operates for more than eleven years.

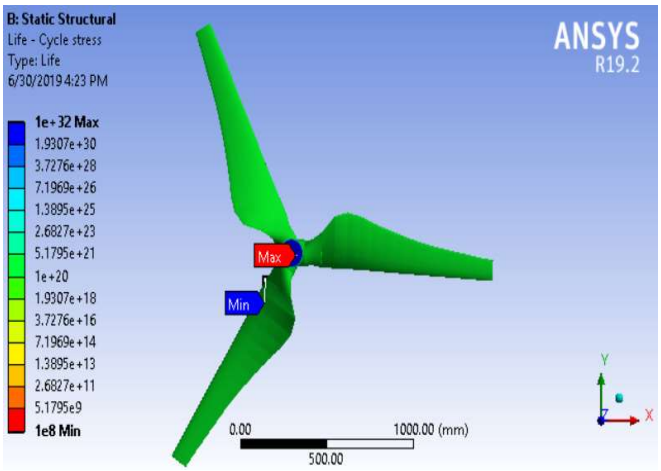

Figure 13 Fatigue life of the blade.

4. Conclusion

Fatigue analysis of wind turbine blade NACA 4412 was performed under a wind speed of 35 m/s. The load value was calculated to perform a stress analysis of the blade. The results were observed from the ANSYS 19.2 in both CFD and static structural analysis. The deformation blade along the span was also studied. After completing both CFD and static structural analysis, the output results such as deformation, stress, and shear stress are identified in static structural. Simultaneously, highly pressurized (critical location) on the blade is shown on CFD results. The factors that are the leading cause of fatigue failure in composite wind turbine blade is identified and determined. High-stress concentration leads to fatigue failure. The life span of the blade length of 1.22 m is approximated for E-glass fibre with a thickness of 5 mm and frame (web) made of aluminium alloy of a thickness of 3 mm. 3-D engineering model of a blade of the wind turbine in this study can operate for a minimum of 11.2 years.

A critical location on the blade where maximum stress was identified, and the comparison between a CFD generated pressure distribution and static structure analysis was performed. The maximum stress location in a wind turbine is the blade's leading edge and the blade root (part the nearer of the hub). As the wind speed increases beyond recommendation design, it decreases the life of the wind turbine blade. The blade's leading edge is more deformed, and the centrifugal load is considered the most influential factor in the life of the blades.

5. References

[1] Gaddada S, Kodicherla SPK. Wind energy potential and cost estimation of wind energy conversion systems (WECSs) for electricity generation in the eight selected locations of Tigray region (Ethiopia). Renew Wind Water Sol. 2016;3(1):2-13.

[2] Kumar KS, Kumar MA, Nanduri PM. Analysis of wind speed data for energy production at Central Ethiopia, Adama. IJLRET. 2015;1(2):1-8.

[3] Mulugeta B, Gerawork A. Aerodynamic design of horizontal axis wind turbine blades. FME Trans. Epub ahead of print. FME Transactions. 2017;45(4):647-660.

[4] Grujicic M, Arakere G, Subramanian E, Sellappan V, Vallejo A, Ozen M. Structural-response analysis, fatigue-life prediction, and material selection for 1 MW horizontal-axis wind-turbine blades. J Mater Eng Perform. 2010;19(6):790-801.

[5] Tawade SV, Todkar SB, Hade AS. Fatigue life optimization of wind turbine blade. Int J Res Eng Technol. 2014;3(3):843-850.

[6] Lin JH, Xu YL, Xia Y. Structural analysis of large-scale vertical axis wind turbines Part II: fatigue and ultimate strength analyses. Energies. 2019;12(13):2584.

[7] Ismaiel AM, Metwalli SM, Elhadidi BM, Yoshida S. Fatigue analysis of an optimized HAWT composite blade. Evergreen. 2017;4(2-3):1-6.

[8] Sardi HE, Sankararaman S, Escobet T, Puig VC, Frost SA, Goebel K. Analysis of two modeling approaches for fatigue estimation and remaining useful life predictions of wind turbine blades. In: Orchard M, editor in chief. Third European Conference of the Prognostics and Health Management Society; 2016 Jul 5-8; Bilbao, Spain. New York: PHM Society; 2009. p. 1-11.

[9] Hu W, Choi KK, Cho HK. Reliability-based design optimization of wind turbine blades for fatigue life under dynamic wind load uncertainty. Struct Multidiscipl Optim. 2016;54(4):953-970.

[10] Lambert J, Chambers AR, Sinclair I, Spearing SM. 3D damage characterisation and the role of voids in the fatigue of wind turbine blade materials. Compos Sci Technol. 2012;72(2):337-343.

[11] Kulkarni PA, Hu WF, Dhoble AS, Padole PM. Statistical wind prediction and fatigue analysis for horizontal-axis wind turbine composite material blade under dynamic loads. Adv Mech Eng. 2017;9(9):1-26.

[12] Lee HG, Park JS. Static test until structural collapse after fatigue testing of a full-scale wind turbine blade. Compos Struct. 2016;136:251-257.

[13] Gonabadi H, Moharrami N, Oila A, Bull SJ. Wet flexural fatigue behaviour of tidal turbine blade composite materials. In: Hoffmann F, editor. 11th European Wave and Tidal Energy Conference; 2015 Sep 6-11; Nantes, France. Newcastle: ePrints; 2003. p. 1-11.

[14] Mahri ZL, Rouabah MS. Calculation of dynamic stresses using finite element method and prediction of fatigue failure for wind turbine rotor. WSEAS Trans Appl Theor Mech. 2008;3(1):28-41.

[15] Chen HP, Zhang C, Huang TL. Stochastic modelling fatigue crack evolution and optimum maintenance strategy for composite blades of wind turbines. Struct Eng Mech. 2017;63(6):703-712.

[16] Castro O, Lennie M, Branner K, Pechlivanoglou G, Brøndsted P, Mayeri CN, et al. Comparing fatigue life estimations of composite wind turbine blades using different fatigue analysis tools. In: Thomsen OT, editor. 20th International Conference on Composite Materials; 2015 Jul 19-24; Copenhagen, Denmark. Ottawa: ICCM; 1975. p. 1-13.

[17] Samborsky DD, Sears AT, Mandell JF. Static and fatigue testing of thick adhesive joints for wind turbine blades. In: Hand MR, editor. 47th AIA Aerospace Sciences meeting including the New Horizons Forum and Aerospace Exposition; 2009 Jan 5-8; Florida, United States. Virginia: AAIA; 1963. p. 1-21.

[18] Leian Z, Xuemei H, Guangming Y. Fatigue life evaluation for wind turbine blade based on multistage loading accumulative damage theory. Mech Eng J. 2015;9:422-427.

[19] Zhang C, Chen HP. Optimum maintenance strategy for fatigue damaged composite blades of offshore wind turbines using stochastic modelling. In: Chen D, Cho MG, Bargmann S, Choi CK, editors. The 2016 World Congress on Advances in Civil, Environmental, and Materials Research (ACEM16)/The 2016 Structures Congress (Structures16); 2016 Aug 28 - Sep 1; Jeju, South Korea. Daejeon: Techno-Press; 1999. p 1-20.

[20] Fraisse A, Brøndsted P. Compression fatigue of wind turbine blade composite materials and damage mechanism. In: Du SY, Leng JS, editor. 21st International Conference on Composite Materials (ICCM-21); 2017 Aug 20-25; Xi'an, China. Beijng: CSCM; 1989. p. 1-8.

[21] Maldhure SS, Kharde YR. Fatigue failure analysis of small wooden wind turbine blade. Int J Comput Eng Sci. 2013;3(2):58-61.

[22] Tenguria N, Mittal ND, Ahmed SR. Structural analysis of horizontal axis wind turbine blade. Wind Struct An Int J. 2013;16(3):241-248.

[23] Mathew AP, Athul S, Barath P, Rakesh S. Structural analysis of composite wind turbine blade. Int Res J Eng Technol. 2018;5(6):1377-1388.
[24] Rashedi A, Sridhar I, Tseng K. Multi-objective material selection for wind turbine blade and tower: Ashby's approach. Mater Des. 2012;37:521-532.
[25] Kadve A, Sharma P, Patel A. Review on CFD analysis on aerodynamic design optimization of wind turbine rotor blade. Int J Innov Emerg Res Eng. 2016;3(5):178-182.
[26] Dai JC, Hu W, Shen XB. Load and dynamic characteristic analysis of wind turbine flexible blades. J Mech Sci Technol. 2017;31(4):1569-1580.